American Journal of Case Reports

ISSN 1941-5923
© Am J Case Rep, 2014; 15: 404-410
DOI: 10.12659/AJCR.891224

Received: 2014.06.19
Accepted: 2014.06.28
Published: 2014.09.22

Burkitt Lymphoma with Initial Clinical Presentation due to Infiltration of the Central Nervous System and Eye Orbits

Authors' Contribution:
Study Design A
Data Collection B
Statistical Analysis C
Data Interpretation D
Manuscript Preparation E
Literature Search F
Funds Collection G

BDEFG 1,2 Gustavo Bittencourt Camilo
BD 1,2 Dequitier Carvalho Machado
BD 2 Celso Estevão de Oliveira
DE 2 Letícia da Silva Lacerda
BDEFG 2 Romulo Varella de Oliveira
DE 3 Monique de França Silva
BDEFG 1 Agnaldo José Lopes

1 Postgraduate Program in Medical Sciences, State University of Rio de Janeiro, Rio de Janeiro, Brazil
2 Department of Radiology, State University of Rio de Janeiro, Rio de Janeiro, Brazil
3 Department of Anatomic Pathology, State University of Rio de Janeiro, Rio de Janeiro, Brazil

Corresponding Author: Agnaldo José Lopes, e-mail: agnaldolopes.uerj@gmail.com
Conflict of interest: None declared

Patient: Male, 17
Final Diagnosis: Burkitt lymphoma
Symptoms: Anisocoria • ipsilateral ptosis • opthalmoparesis • paresis
Medication: —
Clinical Procedure: —
Specialty: Oncology

Objective: Unusual clinical course

Background: Burkitt lymphoma rarely affects the central nervous system and ocular region. Under these conditions, computed tomography and (particularly) magnetic resonance imaging of the skull increase the diagnostic accuracy, as they objectively show the topography of lesions and the effect of neoplasia on structures.

Case Report: We report here the case of a 17-year-old male whose initial clinical manifestations were related to neurological impairment and to the ocular musculature and ocular innervation. The diagnosis of Burkitt lymphoma with leukemization and infiltration of the central nervous system was confirmed.

Conclusions: In this case, it is important to recognize that the neuroimaging findings were fundamentally important in indicating the initial form of the disease and in directing the appropriate clinical management.

MeSH Keywords: Burkitt Lymphoma • Central Nervous System • Magnetic Resonance Imaging • Orbital Diseases • Tomography, Spiral Computed

Full-text PDF: http://www.amjcaserep.com/abstract/index/idArt/891224

Background

Burkitt lymphoma is a highly proliferative neoplasm derived from undifferentiated lymphocytic cells [1]. This neoplasm is extremely infrequent, and, together with Burkitt-like forms, accounts for only 3–5% of non-Hodgkin lymphomas in immunocompetent adults [2]. Although rare, Burkitt lymphoma affects children more frequently, accounting for 30–50% of pediatric lymphomas in some studies [1]. We report here the case of an adolescent presenting with Burkitt lymphoma displaying an atypical localization in neuroimaging exams.

Case Report

A 17-year-old male without any known immunodeficiencies or comorbidities developed paresthesia and paresis of the right lower limb over a period of 3 months, which progressively worsened. He developed anisocoria due to right eye mydriasis, ophthalmoparesis and ipsilateral palpebral ptosis over 1 week and was then referred for neurological monitoring for photophobia.

The patient was admitted to our hospital with worsening paresthesia, severe headache, vomiting, and lipothymia. He was slightly pale, presenting with mydriatic pupils, ophthalmoplegia of the right eye (cranial nerve III) and ophthalmoparesis of the left eye (cranial nerve VI), palpebral ptosis of the right eye, and paresis of the right lower limb. These clinical manifestations were consistent with compression of the mesencephalic tegmentum, and a computed tomography (CT) scan of the head was then requested, which revealed bilateral and symmetric thickening in the topography of the third cranial nerve, with high uptake of contrast medium (Figure 1). This lesion extended to Meckel's cave, cavernous sinus, and superior orbital fissures and to the apices and lower portions of the eye sockets, being more evident in the right eye (Figure 2). Also observed were the thickening and high uptake of the pituitary stalk and a small ill-defined lytic lesion in the greater wing of the sphenoid bone, extending to the orbit, pachymeninx, and temporal muscles. The main diagnoses then suggested were tuberculosis, sarcoidosis, lymphoma, and abscess.

Laboratory tests were performed, which showed nonspecific changes. Empirical treatment for central nervous system (CNS) tuberculosis and meningitis of the cranial base was begun. Magnetic resonance imaging (MRI) of the skull and eye orbits showed bilateral thickening of the extraocular muscles, isointense in all sequences, in addition to elongated tissue with increased uptake of contrast medium in the topography of the right oculomotor nerve, thickening of the left perimesencephalic cistern, and bilateral obliteration of Meckel's cave (Figures 3–6). A lumbar puncture showed clear and transparent cerebrospinal fluid that was smear-positive for malignant cells and lymphomatous infiltration. The tuberculin skin test result was non-reactive.

Figure 1. Axial CT section of the head after injection of iodinated contrast medium. There is thickening of the oculomotor nerves (arrows) and of the left trigeminal nerve (arrowhead). Thickening of the right superior rectus muscle is also observed (asterisk).

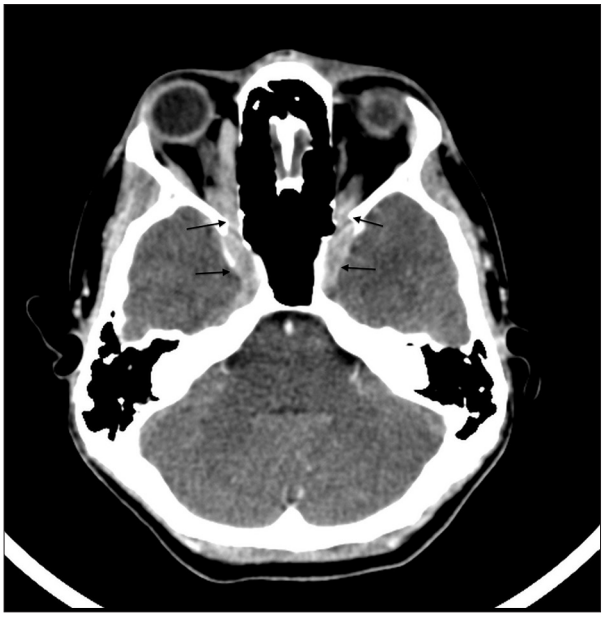

Figure 2. Axial CT section of the head after injection of iodinated contrast medium. This is bilateral thickening of Meckel's cave and cavernous sinuses. An extension of the lesions to the superior orbital fissures and orbital apices is also observed (arrows).

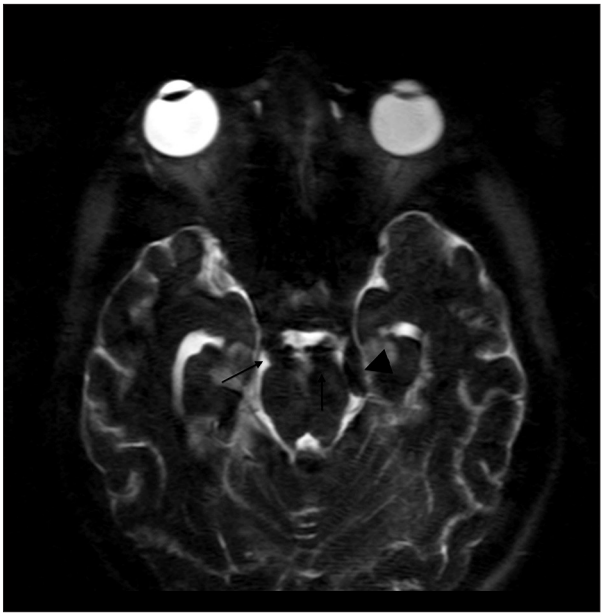

Figure 3. Axial MRI section with 3-dimensional T2-weighted sequence. There is thickening of the oculomotor nerves (arrows) and left trigeminal nerve (arrowhead).

Figure 4. Axial MRI section with T2-weighted sequence and fat suppression. There is thickening of the superior orbital fissures. Extension of the lesions into the orbit and infiltration of the medial rectus muscles (arrows), especially in the right eye, are also observed.

Subsequently, the patient developed intestinal constipation and abdominal pain, and a CT scan of the abdomen and pelvis revealed mild ascites, discrete homogeneous splenomegaly, and 2 lesions located in the pancreas that were hypodense and exhibited increased uptake of contrast medium,

Figure 5. Axial MRI section with T1-weighted sequence with fat suppression after administration of paramagnetic contrast medium. There is high uptake of the contrast medium in the changes described in Figures 3 and 4 (arrows).

Figure 6. Axial MRI section with T1-weighted sequence with fat suppression after administration of paramagnetic contrast medium. There is high uptake of the contrast medium in the lesions in the cavernous sinus and Meckel's cave (arrows). High uptake is also observed in the lesion in the hypothalamus (arrowhead).

resulting in dilatation of the main pancreatic duct and occlusion of the splenic vein with epigastric collateral circulation

Figure 7. Axial CT section of the abdomen after injection of iodinated contrast medium during the portal phase. There are solid lesions with homogeneous enhancement from the contrast medium in the pancreas (arrows) and right kidney (arrowhead). Ectasia of the main pancreatic duct (asterisk) is also observed.

Figure 8. Axial CT section of the abdomen after injection of iodinated contrast medium during the portal phase. There are solid lesions in the head of the pancreas (arrow) and in the transverse colon (asterisk). Gastroepiploic collateral circulation (arrowheads) due to involvement of the splenic vein is also observed.

(Figures 7 and 8). The abdominal CT scan revealed irregular wall thickening in the stomach, jejunum, ileum, cecum, and transverse colon, with signs of intussusception at the ileal lesion (Figures 9–12). Confluent mesenteric lymphadenomegaly next to the jejunal lesion (Figure 10) and hypodense lesions in the right kidney (Figure 7).

The patient developed hematemesis and hemodynamic instability, requiring emergency gastrointestinal endoscopy, whose

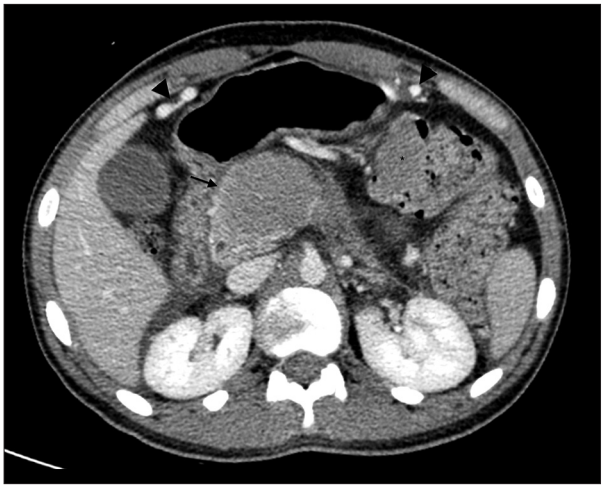

Figure 9. Axial CT section of the abdomen after injection of iodinated contrast medium during the portal phase. There is parietal thickening in the stomach, in addition to ulceration (arrow).

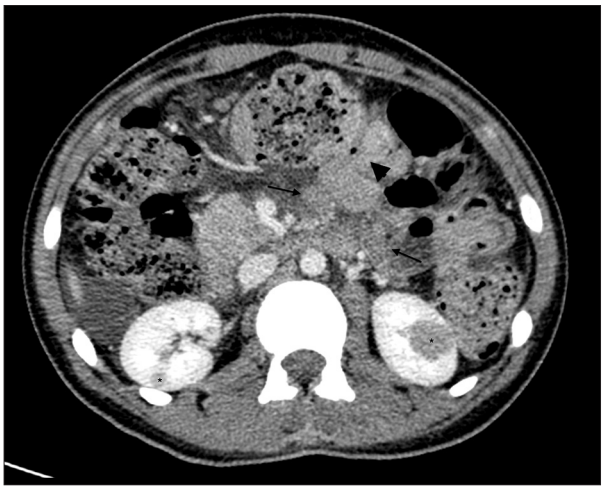

Figure 10. Axial CT section of the abdomen after injection of iodinated contrast medium during the portal phase. There is a mesenteric lymph node conglomerate (arrows) associated with the parietal thickening of the jejunum (arrowhead). Solid renal lesions (asterisks) are also observed.

histopathological finding identified an infiltrative and ulcerated gastric lesion. Hemostasis was performed, and material was collected for biopsy, which revealed Burkitt lymphoma (Figures 13 and 14). A bone marrow biopsy showed the bone marrow to be diffusely infiltrated with blasts, consistent with acute leukemia. The diagnosis of Burkitt lymphoma with leukemization and infiltration of the CNS was then confirmed. The treatment for CNS tuberculosis and meningitis was discontinued, and intrathecal and systemic chemotherapy was initiated. The patient presented with neutropenia and fever, which were treated with cefepime for 11 days. He recovered

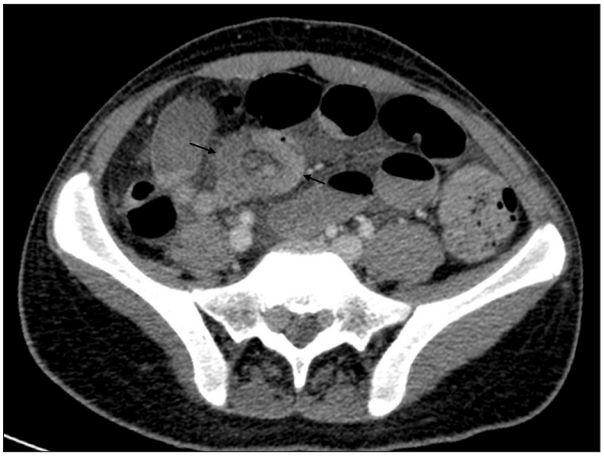

Figure 11. Axial CT section of the abdomen after injection of iodinated contrast medium during the portal phase. 'Targeted' aspect in ileal loop (arrows) is observed, suggesting intestinal intussusception.

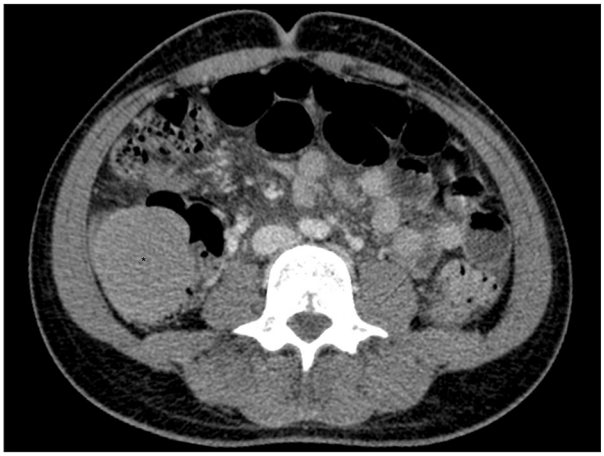

Figure 12. Axial CT section of the abdomen after injection of iodinated contrast medium during the portal phase. A solid lesion in the cecum (asterisk) is observed.

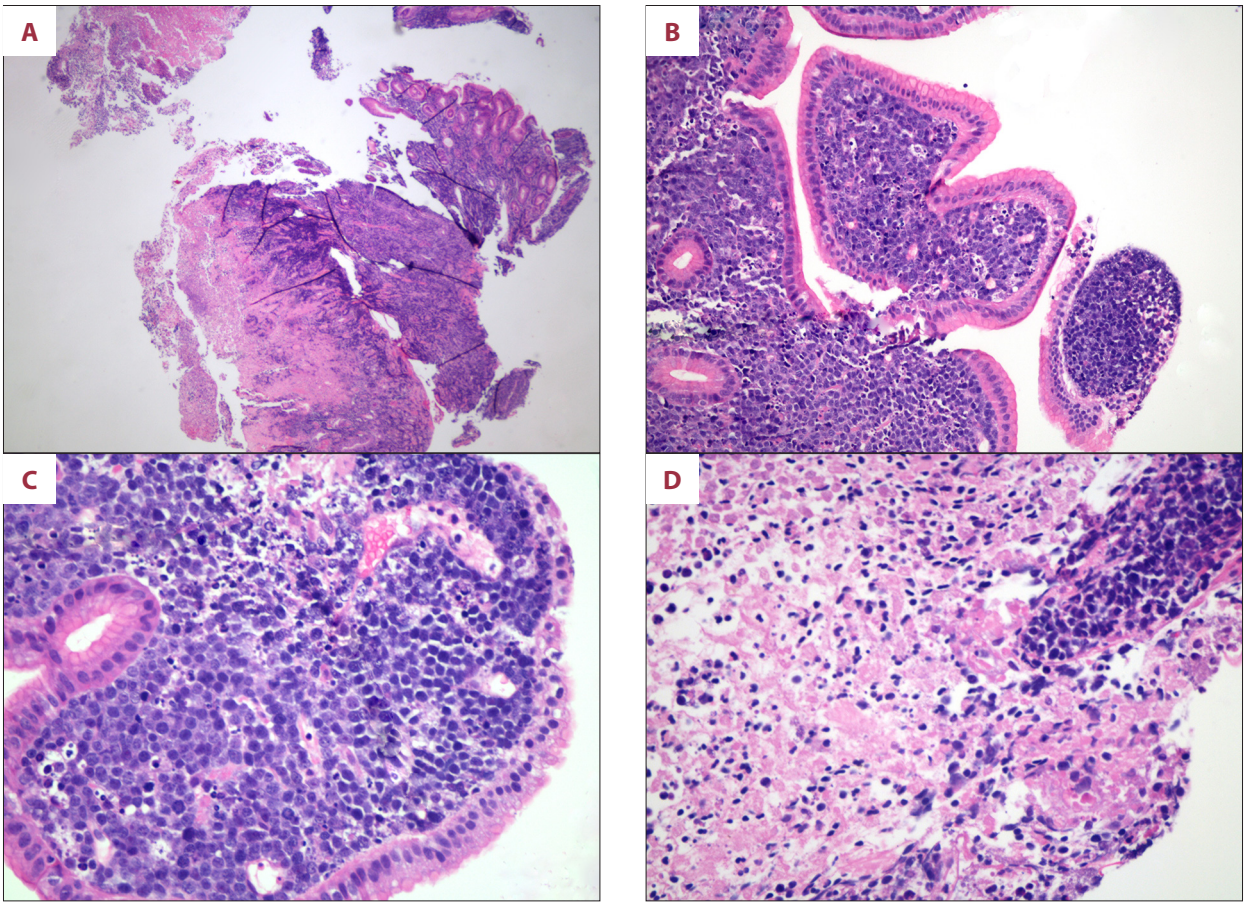

Figure 13. Gastric biopsy (H&E). Corium the gastric mucosa (**A**) filled with diffuse proliferation of round blue cells (**B**). (**C**) Neoplasm of round, blue cells filling the corium. There is molding of the cells as well as pictures of apoptosis default setting of 'starry sky'. (**D**) There is an area of tumor necrosis, reflecting the aggressiveness of the cancer.

satisfactorily and was discharged 2 months after hospitalization with the disease in remission.

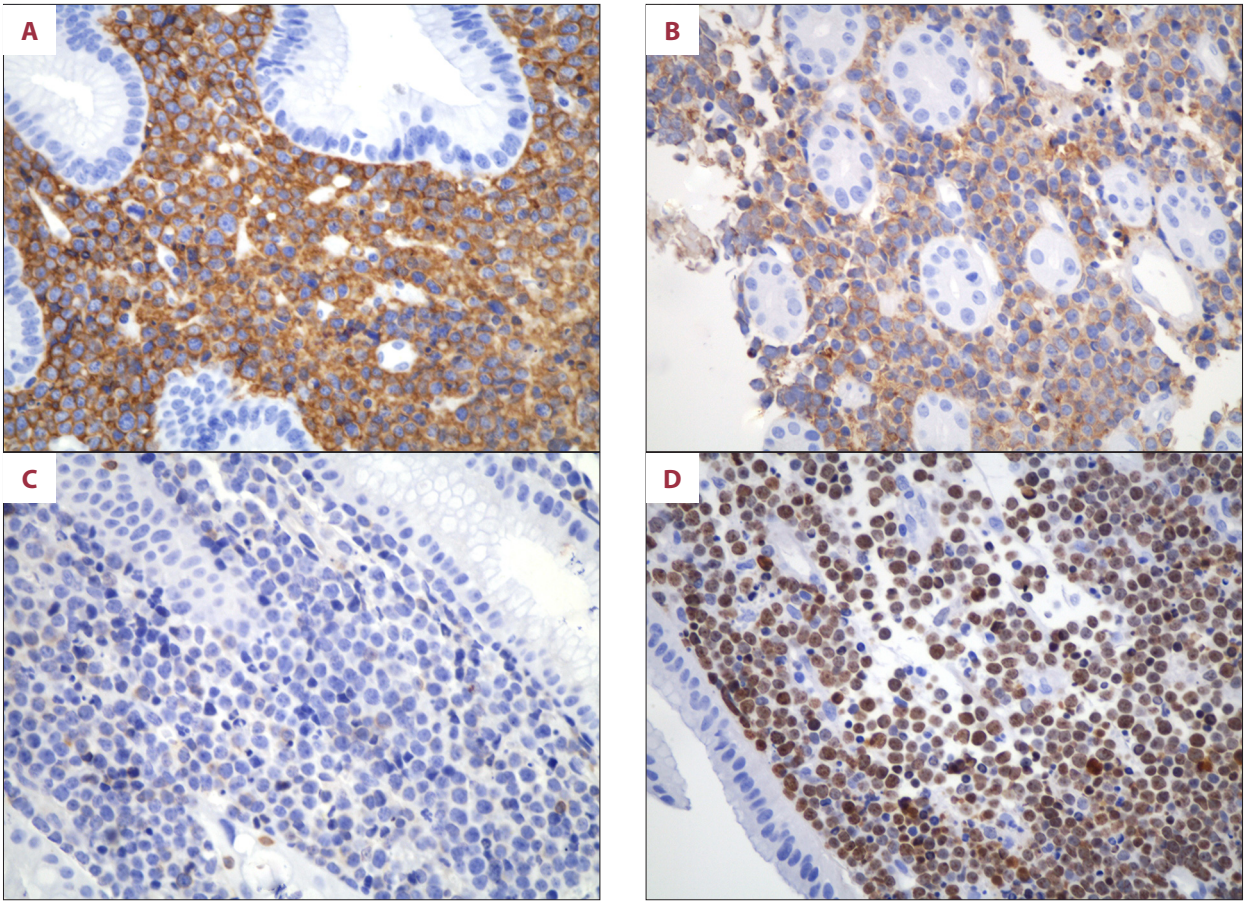

Figure 14. (**A**) Immunohistochemical marker CD20 in neoplastic cells (a marker of B lineage lymphocytes). (**B**) Immunohistochemical marker CD10 in neoplastic cells (a marker of germ cell tumors and lymphomas). (**C**) bcl-2: focal and weak positivity in scattered neoplastic cells (a marker for differentiation with other B-cell lymphomas of high-grade). (**D**) Ki67 >90%, which is expected in Burkitt lymphoma (a marker of cell proliferation, reflecting the aggressiveness of the cancer).

Discussion

Burkitt lymphoma is the most common form of pediatric non-Hodgkin lymphoma. It has 3 main recognized variants: the endemic form, which occurs mostly in equatorial Africa and is strongly associated with the Epstein-Barr virus; the sporadic form, which occurs worldwide; and the form associated with immunodeficiency, primarily in individuals infected with the human immunodeficiency virus [1–7].

Both the sporadic and endemic forms of Burkitt lymphoma present mainly during childhood [8]. The most common sites of involvement are the jaw, facial bones, kidneys, gastrointestinal tract, ovaries, breast, and extranodal sites [9,10]. Abdominal tumors are the most common presentation in sporadic Burkitt lymphoma, whereas mandibular involvement is the most common mode of presentation in the endemic form [10,11].

The involvement of facial bones, including the orbital extension and exophthalmos, are common in the endemic form but rare in the sporadic form, with few cases reported in the literature [12,13]. Burkitt lymphomas primarily involving the brain are extremely rare, with fewer than 10 cases reported in the literature [14–17].

Meningeal involvement and cranial nerve infiltration are the most common CNS presentations of Burkitt and Burkitt-like lymphoma. Meningeal enhancement following intravenous contrast in the T1 sequence of MRI and in a CT scan is the classic finding for this form, but it can be extremely difficult to demonstrate using CT scans [2]. Suprasellar and parasellar tumors that simulate Tolosa-Hunt Syndrome have also been described. An expansive epidural mass with compression on the vertebral canal is the most common presentation of spinal canal involvement [18,19].

MRI is more sensitive in visualizing the involvement of brain lesions and the head and neck [2]. Extracranial head and neck lymphomas tend to present as isointense muscle lesions in the T1 and T2 MRI sequences and with intense and homogeneous

uptake of the intravenous contrast medium. The lesions can be permeative and have foci of bone destruction, suggesting malignant lesions with aggressive behavior [13,20].

The imaging findings for Burkitt lymphoma are non-specific, and in addition to other histological types of lymphoma, the differential diagnosis should include malignant neoplasms with rapid cell proliferation and similar signal characteristics in MRI, such as leukemic infiltration, metastatic neuroblastoma, and sarcoma. Plasmacytomas should also be considered, including cases with bone involvement [13]. Due to their multisystemic involvement and epidemiological importance, we also initially considered sarcoidosis and tuberculosis in the differential diagnosis.

In this case, empirical treatment for CNS tuberculosis was initiated even before the diagnosis of Burkitt lymphoma. The empirical treatment was based on clinical and epidemiological data because our region has a high prevalence of tuberculosis. It is also worth noting the delay in performing lumbar puncture. It is important to identify patients who are at risk of cerebral herniation, in which a lumbar puncture would be contraindicated. The clinical features that suggest raised intracranial pressure include papilledema, focal neurology, and reduced consciousness levels [21]. Importantly, our patient had focal neurology and photophobia, in which papilledema is a difficult sign to detect [22]. Thus, we opted to perform a CT scan of the head prior to lumbar puncture.

Conclusions

We describe a rare initial presentation of Burkitt lymphoma. The lesions started in the CNS and ocular region. Subsequently, the patient had multisystem involvement. Thus, we emphasize the need to explore neuroimaging methods that may indicate the initial form of the disease and guide appropriate clinical management.

References:

1. Dunleavy K, Pittaluga S, Shovlin M et al: Low-intensity therapy in adults with Burkitt's lymphoma. N Engl J Med, 2013; 369(20): 1915–25
2. Johnson KA, Tung K, Mead G, Sweetenham J: The imaging of Burkitt's and Burkitt-like lymphoma. Clin Radiol, 1998; 53(11): 835–41
3. Schmitz R, Young RM, Ceribelli M et al: Burkitt lymphoma pathogenesis and therapeutic targets from structural and functional genomics. Nature, 2012; 490(7418): 116–20
4. Taub R, Moulding C, Battey J et al: Activation and somatic mutation of the translocated c-myc gene in Burkitt lymphoma cells. Cell, 1984; 36(2): 339–48
5. García-Barredo R, Fernández Echevarría MA, del Riego M, Canga A: Soft tissue Burkitt's lymphoma: radiological findings. Eur Radiol, 1998; 8(9): 1654–56
6. Claudi R, Viola P, Cotellese R, Angelucci D: Atypical primary Burkitt lymphoma of the thyroid gland: A practical approach for differential diagnosis and management. Am J Case Rep, 2010; 11: 254–57
7. McClain KL: Non-Hodgkin's lymphoma. In: Principles and Practice of Pediatrics. Oski FA (ed.), 2nd ed. Philadelphia: Lippincott; 1994; 1718–19
8. van den Bosch CA: Is endemic Burkitt's lymphoma an alliance between three infections and a tumour promoter? Lancet Oncol, 2004; 5(12): 738–46
9. Cuadra-Garcia I, Proulx GM, Wu CL et al: Sinonasal lymphoma: a clinicopathologic analysis of 58 patients from the Massachusetts General Hospital. Am J Surg Pathol, 1999; 23(11): 1356–69
10. Upile T, Jerjes W, Abiola J et al: A patient with primary Burkitt's lymphoma of the postnasal space: case report. Head Neck Oncol, 2012; 4: 33
11. Grewal JS, Gunaratnam NT, Krauss JC, Smith LB: Unusual case of Burkitt lymphoma with thyroid gland and abdominal involvement. Am J Case Rep, 2010; 11: 16–19
12. Kalina P, Black K, Waldenberg R: Burkitt lymphoma of the skull base presenting as cavernous sinus syndrome. Pediatr Radiol, 1996; 26(6): 416–17
13. Morriss MC, Friedman DP: Neuroradiology case of the day. Radiographics, 1998; 18(5): 1314–17
14. Valsamis MP, Levine PH, Rapin I et al: Primary intracranial Burkitt's lymphoma in an infant. Cancer, 1976; 37(3): 1500–7
15. Kobayashi H, Sano T, Ii K, Hizawa K: Primary Burkitt-type lymphoma of the central nervous system. Acta Neuropathol, 1984; 64(1): 12–14
16. Hegedus K: Burkitt-type lymphoma and reticulum-cell sarcoma. An usual mixed form of two intracranial primary malignant lymphomas. Surg Neurol, 1984; 21(1): 23–29
17. Monabati A, Rakei SM, Kumar P et al: Primary Burkitt lymphoma of the brain in an immunocompetent patient. J Neurosug, 2002; 96(6): 1127–29
18. Dechambenoit G, Piquemal M, Giordano C et al: Spinal cord compression resulting from Burkitt's lymphoma in children. Child Nerv Syst, 1996; 12(4): 210–14
19. Sanchez Pina C, Pascual-Castroviejo I, Martinez Fernàndez V et al: Burkitt's lymphoma presenting as Tolosa-Hunt syndrome. Pediatr Neurol, 1993; 9(2): 157–58
20. Hudgins PA, Jacobs IN, Castillo M: Pediatric airway disease. In: Head and Neck Imaging. Som PM, Curtin HD (eds.), 3rd edition. St Louis: Mosby-YearBook; 1996; 545–611
21. Cabral DA, Flodmark O, Farrell K, Speert DP: Prospective study of computed tomography in acute bacterial meningitis. J Pediatr, 1987; 111(2): 201–5
22. Nagra I, Wee B, Short J, Banerjee AK: The role of cranial CT in the investigation of meningitis. JRSM Short Rep, 2011; 2(3): 20